Cell Reports

Brain erythropoietin fine-tunes a counterbalance between neurodifferentiation and microglia in the adult hippocampus

Graphical abstract

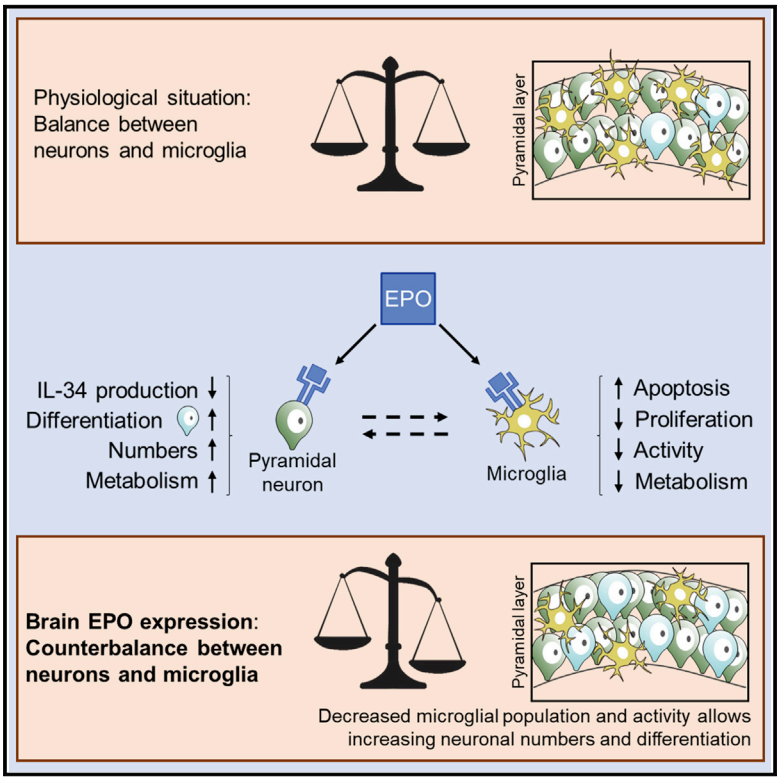

Highlights

- Microglia transiently respond to EPO by apoptosis, followed by abridged proliferation
- Reduction of microglia allows undisturbed fast differentiation of immature neurons
- Microglial and pyramidal EPOR are critical for neurodifferentiation in CA1 on EPO
- EPO acts as regulator of neuronally expressed IL-34 and CSF1R-dependent microglia

Authors

Laura Fernandez Garcia-Agudo, Agnes A. Steixner-Kumar, Yasmina Curto, ..., Juan Nacher, Klaus-Armin Nave, Hannelore Ehrenreich

Correspondence

ehrenreich@em.mpg.de

In brief

Fernandez Garcia-Agudo et al. report prominent EPO effects on neurodifferentiation that depend on a counterbalance between microglia and neurons. Microglia respond to EPO by transient apoptosis followed by dampened activity and reduced proliferation, allowing undisturbed differentiation of immature neuronal subpopulations. This ultimately results in increased numbers of mature hippocampal neurons.

Fernandez Garcia-Agudo et al., 2021, Cell Reports *36*, 109548
August 24, 2021
https://doi.org/10.1016/j.celrep.2021.109548

Cell Reports

CellPress
OPEN ACCESS

Report

Brain erythropoietin fine-tunes a counterbalance between neurodifferentiation and microglia in the adult hippocampus

Laura Fernandez Garcia-Agudo,[1,7] Agnes A. Steixner-Kumar,[1,7] Yasmina Curto,[1,7] Nadine Barnkothe,[1] Imam Hassouna,[1] Sebastian Jähne,[2] Umer Javed Butt,[1] Katharina Grewe,[2] Martin S. Weber,[3] Kim Green,[4] Silvio Rizzoli,[2] Juan Nacher,[5] Klaus-Armin Nave,[6] and Hannelore Ehrenreich[1,8,*]

[1]Clinical Neuroscience, Max Planck Institute of Experimental Medicine, Göttingen, Germany
[2]Department of Neuro- and Sensory Physiology, University Medical Center Göttingen, Göttingen, Germany
[3]Institute of Neuropathology and Department of Neurology, UMG, Göttingen, Germany
[4]Department of Neurobiology and Behavior, Institute for Memory Impairments and Neurological Disorders, University of California, Irvine, Irvine, CA, USA
[5]Neurobiology Unit, Program in Neurosciences and Interdisciplinary Research Structure for Biotechnology and Biomedicine (BIOTECMED), Universitat de València, Burjassot, Spain
[6]Department of Neurogenetics, Max Planck Institute of Experimental Medicine, Göttingen, Germany
[7]These authors contributed equally
[8]Lead contact
*Correspondence: ehrenreich@em.mpg.de
https://doi.org/10.1016/j.celrep.2021.109548

SUMMARY

In adult cornu ammonis hippocampi, erythropoietin (EPO) expression drives the differentiation of new neurons, independent of DNA synthesis, and increases dendritic spine density. This substantial brain hardware upgrade is part of a regulatory circle: during motor-cognitive challenge, neurons experience "functional" hypoxia, triggering neuronal EPO production, which in turn promotes improved performance. Here, we show an unexpected involvement of resident microglia. During EPO upregulation and stimulated neurodifferentiation, either by functional or inspiratory hypoxia, microglia numbers decrease. Treating mice with recombinant human (rh)EPO or exposure to hypoxia recapitulates these changes and reveals the involvement of neuronally expressed IL-34 and microglial CSF1R. Surprisingly, EPO affects microglia in phases, initially by inducing apoptosis, later by reducing proliferation, and overall dampens microglia activity and metabolism, as verified by selective genetic targeting of either the microglial or pyramidal neuronal EPO receptor. We suggest that during accelerating neuronal differentiation, EPO acts as regulator of the CSF1R-dependent microglia.

INTRODUCTION

Erythropoietin (EPO) is a hypoxia-inducible growth factor, expressed in the brain (Brines and Cerami, 2005; Digicaylioglu et al., 1995; Jelkmann, 1992; Marti et al., 1996; Sirén et al., 2009; Suresh et al., 2020). In numerous clinical trials and "back-translational" rodent studies for deeper mechanistic insight, recombinant human (rh)EPO treatment consistently improved cognitive performance, including executive functions, many facets of learning, memory, attention, and processing speed. At the same time, it reduced brain matter loss (Adamcio et al., 2008; Ehrenreich et al., 2007a, 2007b; El-Kordi et al., 2009; Miskowiak et al., 2014, 2015; Sirén et al., 2006; Wustenberg et al., 2011). Searching for underlying mechanisms, we discovered that 3-week rhEPO treatment of mice leads to an ~20% increase in the number of pyramidal neurons and oligodendrocytes in cornu ammonis (CA) hippocampi in the absence of altered cell proliferation or apoptosis (Hassouna et al., 2016; Wakhloo et al., 2020). An equivalent ~20% of neurons showed elevated *de novo* protein production. In EPO-treated NG2-CreERT2 mice, we directly confirmed enhanced differentiation of preexisting oligodendrocyte precursors without elevated DNA synthesis (Hassouna et al., 2016). Regarding neuronal lineages, the picture is much more complex, with EPO apparently driving fast differentiation of diverse, non-dividing, local neuronal precursors (Hassouna et al., 2016; Wakhloo et al., 2020), similar to its established role in the hematopoietic system (Brown and Ceredig, 2019; Dessypris et al., 1988; Grover et al., 2014; Krantz, 1991). Exposure to motor-cognitive challenge, namely complex running wheels (CRW) (Liebetanz and Merkler, 2006), leads to endogenous hypoxia in pyramidal neurons, augmenting the expression of EPO and EPO receptor (EPOR) (Butt et al., 2021a, 2021b; Wakhloo et al., 2020). These in turn prompt via autocrine/paracrine signaling the emergence of newly generated CA neurons, enhance dendritic spine densities, and improve performance (*EPO brain doping*). Single-cell RNA sequencing

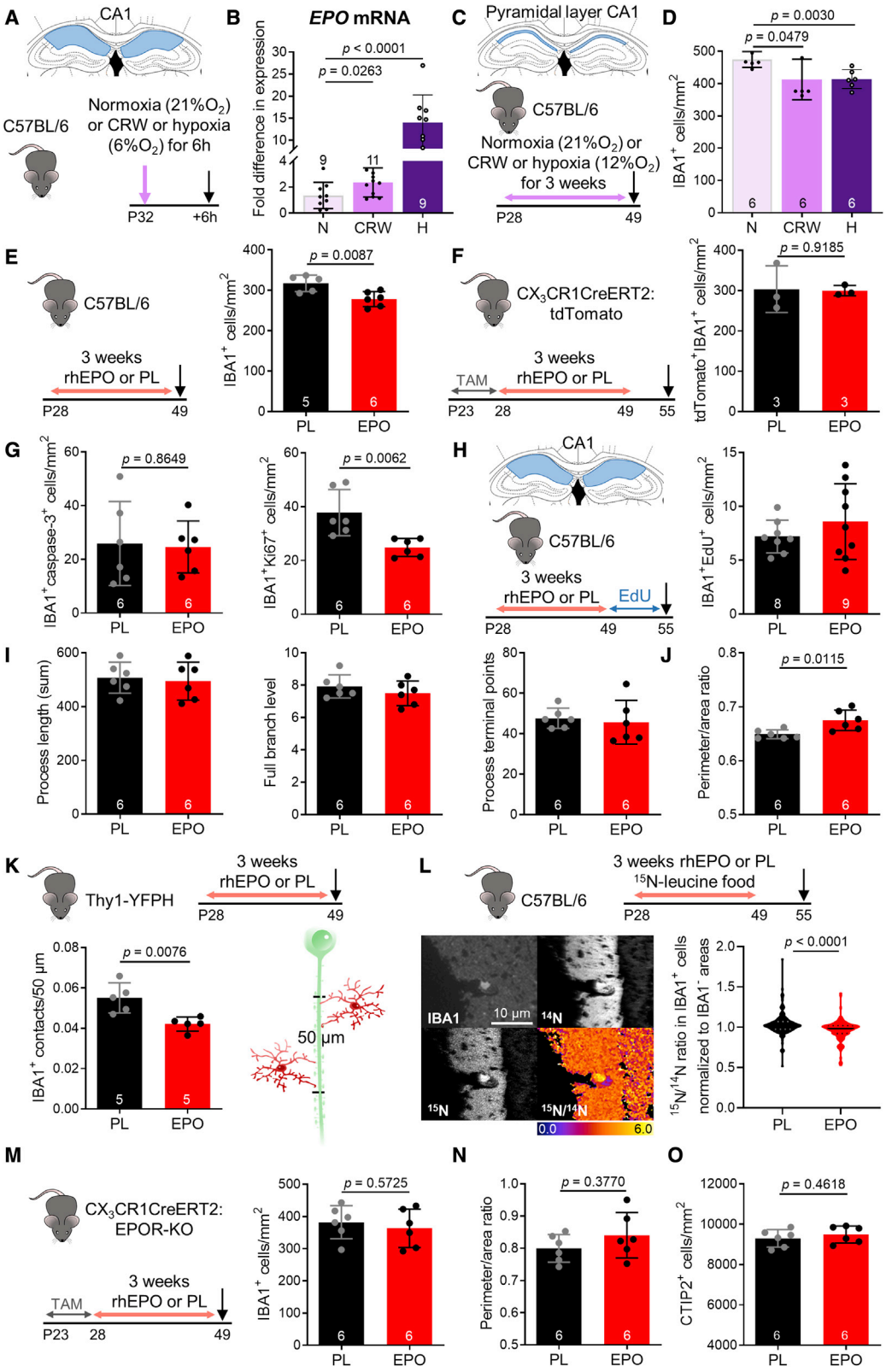

(legend on next page)

(scRNA-seq) in CA1, only 6 h after 1 intraperitoneal rhEPO injection, revealed a rapid increase in newly differentiating neurons. Exposure to either moderate inspiratory hypoxia (12%O_2) or to CRW (*functional hypoxia*) imitated the formation of new pyramidal neurons seen under rhEPO, and inspiratory hypoxia combined with CRW even acted synergistically. All of these effects depend on pyramidal neuronal expression of the EPOR gene (Wakhloo et al., 2020). Thus, a model of neuroplasticity emerged in which neuronal networks, challenged by motor-cognitive tasks, drift into functional hypoxia, which in turn triggers neuronal EPO expression. This regulatory brain EPO circle causes lasting neuroplastic adaptation, which we called *brain hardware upgrade*. Importantly, these EPO-mediated adaptation processes likely also involve other brain cell types that express and/or bind EPO, at least in disease models (Brines and Cerami, 2005; Ott et al., 2015; Sargin et al., 2010; Sirén et al., 2009).

In the physiological context of challenge-induced neuroplasticity, the contribution of microglia is of particular interest, but still entirely unexplored. In fact, microglia have crucial roles in neurotrophic support, neurogenesis, and synaptogenesis, including synaptic and axonal pruning or removal of dying neurons, and are constantly responding to neuronal signals by extending and withdrawing their processes from around synapses (Kierdorf and Prinz, 2017; Werneburg et al., 2017). Thereby, they shape developmental and postnatal neuronal circuits, the latter in an activity-dependent manner. Interestingly, recent work shows that microglia respond to neuronal activation by suppressing neuronal activity in the sense of a microglia-mediated negative feedback mechanism. This mechanism operates similarly to inhibitory neurons, protects the brain from excessive activation, and depends on microglia sensing and catabolizing extracellular ATP that is released upon neuronal activation by neurons and astrocytes (Badimon et al., 2020).

The way, however, in which microglia co-regulate adult neurogenesis, and particularly adult neurodifferentiation in various states of neuronal activation, and outside the classical neurogenesis niches is still poorly understood (Butovsky and Weiner, 2018). The present study has been designed to explore in healthy mice how microglia behave in the context of EPO-mediated ample brain hardware upgrade in hippocampal CA1. Surprisingly, we show that EPO decreases microglia numbers, first by inducing apoptosis, followed by inhibiting proliferation. In parallel, EPO dampens microglia activity and metabolism. This effective containment of microglia is a prerequisite for an undisturbed EPO-driven neuronal differentiation in CA1. It depends on microglial EPOR and involves the colony-stimulating factor 1 receptor (CSF1R) system.

RESULTS AND DISCUSSION

Inspiratory and functional hypoxia induce endogenous EPO expression in brain and diminish microglia numbers in CA1

EPO is a hypoxia-inducible growth factor, swiftly upregulated upon reduced inspiratory oxygen availability or upon relative oxygen deficiency (more oxygen consumed than provided in steady state) in peripheral tissues as well as in brain (Brines and Cerami, 2005; Jelkmann, 1992). We compared by qPCR the EPO expression in CA1 after 6 h of strong exogenous hypoxia (reduced inspiratory oxygen; positive control; 6% O_2) with 6 h of functional hypoxia (i.e., relative oxygen deficiency), induced by using our CRW paradigm of motor-cognitive challenge (Butt et al., 2021a, 2021b; Wakhloo et al., 2020). Under both conditions, *EPO* mRNA expression increased acutely compared to normoxia baseline (Figures 1A and 1B), supporting the next steps toward a more chronic approach.

From our previous work, we know that chronic endogenous EPO induction in the brain by functional and inspiratory hypoxia promotes adult hippocampal neurodifferentiation in CA1, similar to exogenously applied rhEPO (Hassouna et al., 2016; Wakhloo et al., 2020). Here, we wondered how this would reflect on the microglial population dynamics, which in this context have remained unexplored. To elucidate the physiological effect of endogenous brain EPO on microglia, we exposed wild-type (WT) mice, starting at post-natal day 28 (P28), to 3 weeks of CRW versus permanent moderate inspiratory hypoxia (12% O_2; Figure 1C). In both conditions, IBA1$^+$ microglia in CA1 pyramidal layer were reduced immediately after these 3 weeks (P49), compared to normoxia control mice (Figure 1D). Importantly, this reduction was comparable to that obtained after treating WT mice with rhEPO (5,000 IU/kg intraperitoneally [i.p.] every other day for 3 weeks) versus placebo injections (Figure 1E). The

Figure 1. Inspiratory and functional hypoxia induce brain EPO expression and diminish microglia numbers, imitation by rhEPO, and dependence on EPOR

(A and B) Treatment scheme and hippocampal area of analysis (A) for (B) *EPO* mRNA expression (normalized to *Hprt1*) in P32 WT C57BL/6 mice, exposed for 6 h to normoxia (21% O_2; N), functional hypoxia upon CRW performance, or inspiratory hypoxia (6% O_2; H).

(C and D) Scheme for normoxia, CRW, or inspiratory hypoxia (12% O_2), extended to 3 weeks and area of IBA1 quantification (C), given in (D).

(E) IBA1 quantification after 3 weeks of rhEPO or placebo (PL) treatment.

(F) Quantification of tdTomato$^+$IBA1$^+$ cells 1 week after cessation of rhEPO/PL treatment of CX_3CR1CreERT2:tdTomato mice.

(G) Quantification of caspase-3$^+$ and Ki67$^+$ microglia in mice of (E).

(H) Scheme for administration of EdU for 1 week after rhEPO/PL treatment cessation and area/quantification of IBA1$^+$EdU$^+$ cells.

(I) Morphological analysis of microglia processes in mice of (E).

(J) Morphological analysis of microglia cell bodies in mice of (E).

(K) Density of IBA1$^+$ contacts on apical dendrites of Thy1-YFP$^+$ pyramidal neurons after 3 weeks of rhEPO/PL and illustration thereof.

(L) NanoSIMS experiment after ^{15}N-leucine-enriched food, provided for the same 3-week duration as rhEPO/PL (N = 4 mice/group); representative images and calculated ^{15}N/^{14}N ratio in IBA1$^+$ cells as measure of ^{15}N-leucine incorporation (normalized to IBA1$^-$ areas); area of analysis in (A).

(M and N) IBA1 quantification in CX_3CR1CreERT2:EPOR-KO mice after 3 weeks of rhEPO/PL (M), and (N) morphological analysis of microglia cell bodies.

(O) CTIP2$^+$ neuron quantification in mice from (M).

All graphs show means ± SEMs with N numbers in bars and unpaired 2-tailed t tests, except for (L), in which a 2-tailed Mann-Whitney *U* test was performed; analyses conducted in area shown in (C), except as otherwise indicated.

amount of rhEPO reaching the brain in healthy rodents with an intact blood-brain barrier is similar to the endogenously induced brain EPO (Ehrenreich et al., 2004). The decrease in microglia numbers in CA1 simultaneously with increased neurodifferentiation upon EPO (Hassouna et al., 2016; Wakhloo et al., 2020) validated rhEPO treatment as a highly standardizable and convenient model procedure for the present study.

Effect of rhEPO on microglia numbers and activity depends on microglial EPOR

We next asked how long the reduction of microglia numbers seen on P49 (i.e., immediately after cessation of rhEPO treatment) would last. To answer this question and at the same time to use a permanent cell label in addition to IBA1 staining, we treated $CX_3CR1CreERT2$:tdTomato mice for 3 weeks with rhEPO according to our schedule. On P49, the reduction of microglia numbers was reproducible in this mouse line (PL 309.51 ± 20.09 versus EPO 271.45 ± 2.76; n = 4/group; Student's unpaired 2-tailed t test p = 0.0548). Notably, already 1 week later (P55), microglia numbers (all consistently tdTomato$^+$IBA1$^+$) were no longer different from placebo-treated mice (Figure 1F), pointing to a tight and time-limited regulation of microglia under EPO with fast repopulation thereafter. Since all tdTomato$^+$ cells were also IBA1$^+$, the possibility of microglia losing their identity or transdifferentiating to other cell types upon EPO could be discarded.

We thus explored other reasons behind the decreased microglia numbers under rhEPO. On P49, caspase-3 staining revealed no enhanced apoptosis, whereas IBA1$^+$Ki67$^+$ cells were diminished (Figure 1G), also reflected in the ratio of IBA1$^+$Ki67$^+$:IBA1$^+$ microglia (PL 12.29 ± 0.86 versus EPO 8.89 ± 0.34; Student's unpaired 2-tailed t test p = 0.0042). This points to a reduced cell cycle/proliferation of microglia after 3 weeks of rhEPO. Application of 5-ethynyl-2′-deoxyuridine (EdU) for 1 week, starting immediately after rhEPO treatment cessation (P49), disclosed a trend for more proliferating microglia compared to placebo at P55 (Figure 1H), which certainly contributed to the quick recovery of microglia numbers (Figure 1F).

Microglial morphology and their contact with neurons are notorious for accurately reflecting their activity status (Cserép et al., 2021; Sierra et al., 2016). The physical relationship of microglia with neurons is highly relevant, since synaptic stripping or phagocytosis of apoptotic cells are mediated by direct contacts (Cserép et al., 2021). Parameters of microglia process complexity (Figure 1I) did not show differences between rhEPO and placebo groups. However, analysis of the microglia cell body revealed an increased perimeter:area ratio, which is consistent with a less active phenotype (Peskin et al., 2010) upon rhEPO treatment (Figure 1J). The decreased number of contacts per longitude of Thy1-YFP$^+$ pyramidal dendrites further supports the reduced activity of microglia after 3 weeks of rhEPO (Figure 1K), as does an abridged metabolic turnover, measured by ^{15}N-leucine incorporation into IBA1$^+$ cells using NanoSIMS (Figure 1L). This is in contrast to the increased ^{15}N-leucine incorporation in NeuN$^+$ neurons upon rhEPO (Hassouna et al., 2016). Hence, in parallel to the rhEPO-stimulated neurodifferentiation in CA1, resulting in a substantial number of new functional pyramidal neurons with their expectedly enhanced protein turnover reported previously (Hassouna et al., 2016; Wakhloo et al., 2020), we show that microglia are decreased in number, metabolism, and activity. Notably, decreased numbers or functionality of microglia are known to affect neurogenesis and neurodifferentiation in the mouse hippocampus (Diaz-Aparicio et al., 2020; Elmore et al., 2018). Thus, the overall dampening of microglia by EPO detected here is likely prerequisite for the increased neurodifferentiation upon EPO, supporting a two-wire effect of this potent growth factor.

To investigate next whether the effects of rhEPO on microglia depend on microglial EPOR, we selectively erased EPOR in microglia by generating $CX_3CR1CreERT2$:EPOR-KO (knockout) mice. After tamoxifen-induced deletion and subsequent rhEPO treatment following our 3-week schedule, we did not find reduction of microglia numbers or changes in cell body size (Figures 1M and 1N). This supports the direct effects of EPO on microglia that disappear after microglial EPOR elimination. Most important, the earlier reported increase in CTIP2$^+$ CA1 pyramidal neurons upon EPO treatment (Hassouna et al., 2016) was completely absent in these mice (Figure 1O), identifying the simultaneous microglia reduction as a necessary step for EPO-induced increase in pyramidal neurons.

Counterbalance between microglia and newly generated neurons upon EPO

We previously reported EPO to powerfully drive neurodifferentiation, leading to increased numbers of immature or mature neurons, depending on the time point studied (Hassouna et al., 2016; Wakhloo et al., 2020). Since microglia are dampened by EPO, but reportedly crucial for proper neuronal development and differentiation (Hattori et al., 2020; Nandi et al., 2012), we wondered whether, when, and how EPO would provide the physiological counterbalance between neuronal and microglial populations in the neurodifferentiation process. Treating mice for only 1 week with rhEPO or placebo resulted in reduced microglia numbers (Figures 2A and 2B). Notably, at this early time point, caspase-3$^+$ or Ki67$^+$ microglia were unaltered (Figure 2C); however, microglia activity was already reduced (Figure 2D). How was the observed microglia reduction achieved, and could this indicate protection of ongoing neurodifferentiation? We quantified mature CTIP2$^+$ and immature TBR1$^+$ neurons at the 1-week time point, as both are increased in the CA1 pyramidal layer upon rhEPO, the former after 3 weeks and the latter at 24 h (Hassouna et al., 2016; Wakhloo et al., 2020). No differences were seen at 1 week of rhEPO treatment in either population, suggesting that this time point was too early to find mature neurons increased, and too late to still see the initial TBR1 wave of precursors (Figure 2E). We thus hypothesized that after 1 week of rhEPO treatment, newly differentiating neurons would be in an intermediate stage, having further progressed along the maturation path (pseudotime trajectory; Wakhloo et al., 2020), obtained by scRNA-seq of CA1 at 6 h after a single rhEPO injection (Figures 2F and 2G). Whereas TBR1 marks an early immature stage (Figure 2H), we focused on a population of intermediately mature neurons in the pseudotime trajectory (Wakhloo et al., 2020) and selected *Zbtb20* as a marker, highly specific for maturing pyramidal neurons of CA1 (Nielsen et al., 2010, 2014; Xie et al., 2010) (p = 2.31e−63; Figure 2I). Immunohistochemical quantification showed an increased number of

CellPress
OPEN ACCESS

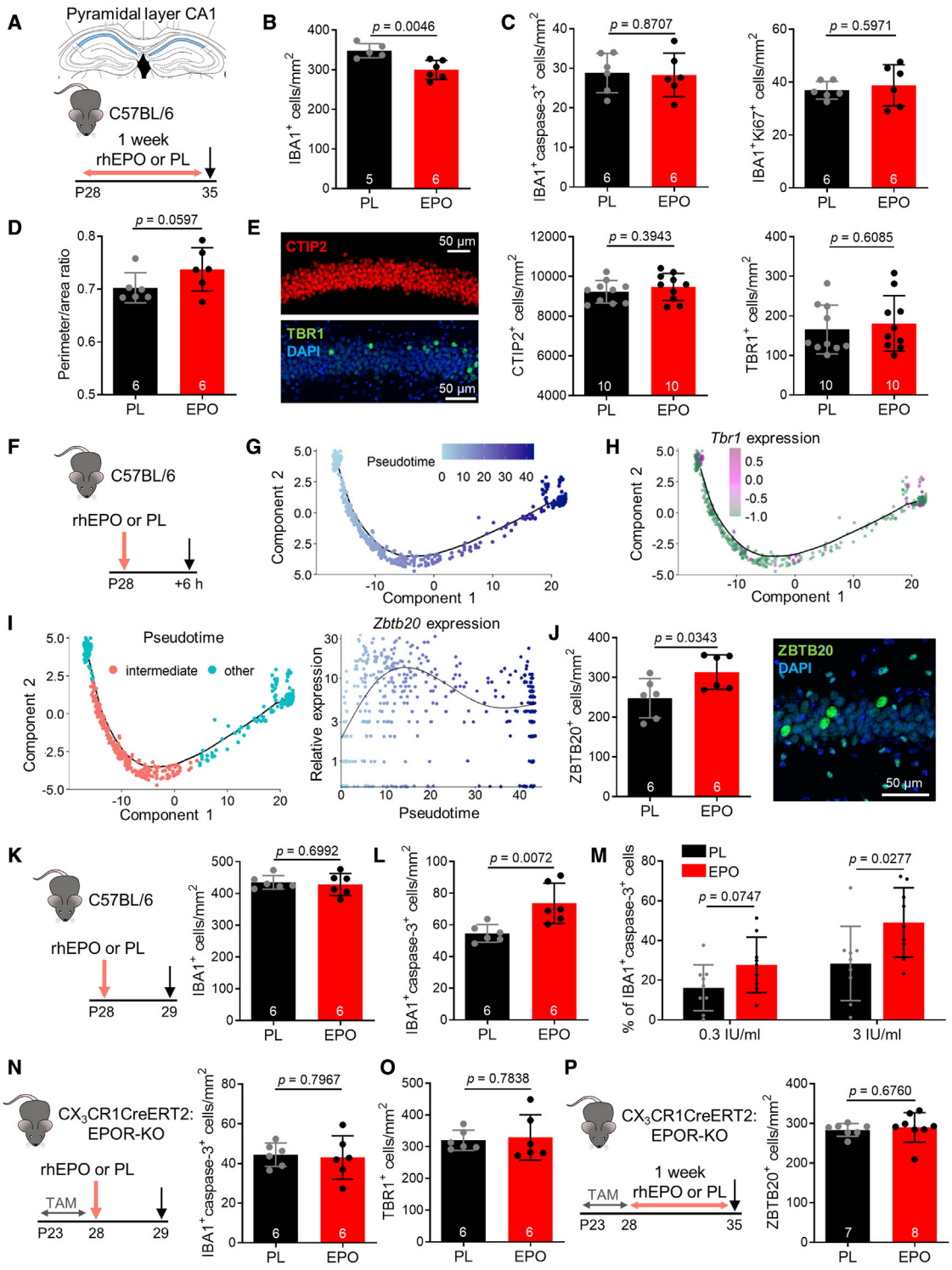

Figure 2. Counterbalance between microglia and newly generated neurons upon EPO

(A–C) Scheme for (A) 1 week of rhEPO/PL treatment in P28 WT C57BL/6 mice and hippocampal area of analysis for (B) IBA1 and (C) quantifications of caspase-3$^+$ and Ki67$^+$ microglia.

(D) Morphological analysis of microglia cell bodies.

(E) Representative images and quantifications of cells with neuronal markers CTIP2 and TBR1.

(F) scRNA-seq analysis after 6 h of single rhEPO/PL injection.

(legend continued on next page)

ZBTB20$^+$ cells in the CA1 pyramidal layer after 1 week of rhEPO (Figure 2J), confirming the ongoing wave of stimulated neurodifferentiation. This temporary ZBTB20 surge was not yet visible at the 24-h time point (ZBTB20$^+$ cells/mm^2: PL 275.08 ± 19.29 versus EPO 295.38 ± 13.73; N = 5/group; Student's unpaired 2-tailed t test p = 0.4316) and found to be terminated already at 3 weeks of rhEPO treatment (ZBTB20$^+$ cells/mm^2: PL 531.5 ± 28.25 versus EPO 497.25 ± 38.75; N = 4/group; Student's unpaired 2-tailed t test p = 0.5019). These data indicate that upon EPO, the individual neurodifferentiation markers in CA1 rise only at particular time windows, as nicely predicted by the pseudotime course.

Apoptosis as a mechanism explaining the EPO-induced reduction in microglia

To elucidate the mechanisms that could have led to the observed reduction of IBA1$^+$ cells after 1 week of rhEPO, we next quantified microglia at 24 h after a single rhEPO or placebo injection. At this early time point, no difference in IBA1$^+$ cells yet appeared (Figure 2K), but, surprisingly, the number of caspase-3$^+$ microglia was elevated in rhEPO-treated mice (Figure 2L). As EPO is usually associated with a strong anti-apoptotic role (Krantz, 1991; Sirén et al., 2001) and has pro-apoptotic effects only in unphysiologically high doses, at least in neurons (Ehrenreich et al., 2005), we wondered whether such an unexpected consequence of rhEPO would similarly be detectable in primary microglia in culture. Indeed, also, pure microglia cultures revealed a rapid pro-apoptotic function of rhEPO in this cell type, reflected by increased caspase-3 expression after only 6 h (Figure 2M). At the 24-h time point, the enhanced caspase-3 expression in culture had already disappeared (data not shown).

To confirm a direct role of the microglial EPOR in apoptosis induction, we used once more our CX$_3$CR1CreERT2:EPOR-KO mice. The increase in caspase-3$^+$ microglia seen after 24 h of a single rhEPO injection in WT mice (Figure 2L) was abolished in the absence of a functional microglial EPOR (Figure 2N). At this early time point, the numbers of microglia were unchanged also in the absence of EPOR (IBA1$^+$ cells/mm^2: PL 336.8 ± 1.9 versus EPO 343.7 ± 11.29; N = 6/group; Student's unpaired 2-tailed t test p = 0.5601). These data suggest that EPO *in vivo* and *in vitro* quickly and transiently induces the apoptosis of microglia. This temporary apoptosis within the microglia population, prompted by EPO, is in perfect agreement with a 2017 report, showing that microglia self-renewal is maintained by coupled proliferation and apoptosis, resulting in a stable microglia number (Askew et al., 2017). Thus, apoptosis is a physiological regulatory instrument in this cell type next to controlled proliferation, and with our data, we unify these effects to one particular factor, namely EPO, that, via microglial EPOR, mediates these regulating mechanisms in a phasic fashion.

Importantly, we also realized in CX$_3$CR1CreERT2:EPOR-KO mice that the rhEPO-induced increase in TBR1$^+$ precursors/immature neurons at 24 h was eliminated (Figure 2O) and, analogously, at the 1-week time point, the EPO-mediated surge of ZBTB20$^+$ immature neurons was eradicated (Figure 2P). This confirms again that an intact microglial EPOR is instrumental for the observed two-wire effect of EPO on neurodifferentiation. Together with our previous (Hassouna et al., 2016; Wakhloo et al., 2020) and present studies on neurodifferentiation, these data attest to a delicate counterbalance, orchestrated by EPO, between neuronal differentiation and microglia numbers and activity.

Both endogenous and exogenous EPO affect microglial proliferation via CSF1R

We next hypothesized that EPO may interfere with CSF1R that is crucial for microglial proliferation and survival (Elmore et al., 2014). Thus, we depleted brains of microglia by feeding the CSF1R inhibitor PLX5622 to WT mice for 10 days. Immediately after inhibitor withdrawal, when fast microglia repopulation takes place (Dagher et al., 2015), we started our usual 3-week rhEPO treatment, and simultaneously added EdU to the drinking water for the first week. Since we were interested in observing how the neuronal population would respond to this challenge of the neuron-microglia counterbalance, we allowed a 1-week break after rhEPO treatment cessation (Figures 3A and 3B), permitting a fully recovered microglia compartment and following the experimental paradigm that had led earlier to the increase in CTIP2$^+$ neurons of the CA1 pyramidal layer (Hassouna et al., 2016). As expected, we found no changes in the overall IBA1$^+$ cell numbers at the P57 time point (Figure 3C, compare with Figure 1F). However, the EdU$^+$ microglia, marking proliferation during the first week of repopulation, were decreased upon rhEPO by ~50% (Figure 3C). We replicated our previous finding of rhEPO increasing CTIP2$^+$ neuron numbers (Hassouna et al., 2016) (Figure 3D), but, surprisingly, this increase was similarly observed in PLX5622-treated mice, independent of rhEPO. This indicated that in the absence of microglia, the neuronal differentiation advances to reach a ceiling effect, not amplified further by the addition of rhEPO. As shown earlier (Hassouna

(G) Pseudotime trajectory of glutamatergic cells of CA1 (Wakhloo et al., 2020).
(H) *Tbr1* expression along pseudotime trajectory/neuronal maturation stages (Wakhloo et al., 2020); expression indicated as log10(normalized expression+0.1).
(I) Selection of a population of neurons with intermediate maturity and identification of *Zbtb20* as a marker transiently increased during maturation (i.e., highly expressed in this population).
(J) Quantification and representative illustrating image of ZBTB20 in mice from (A).
(K) Scheme for 24 h of rhEPO/PL treatment and IBA1 quantification in these mice.
(L) Quantification of IBA1$^+$caspase-3$^+$ microglia in mice from (K).
(M) IBA1$^+$caspase-3$^+$ cells in pure microglia cultures after 6 h of rhEPO/PL addition; *in vitro* data represent triplicate measurements from 3 independent cultures (biological replicates).
(N) IBA1$^+$caspase-3$^+$ microglia quantification in CX$_3$CR1CreERT2:EPOR-KO mice, sacrificed 24 h after 1 rhEPO/PL injection.
(O) TBR1$^+$ immature neuron quantification in mice from (N).
(P) ZBTB20$^+$ immature neuron quantification in CX$_3$CR1CreERT2:EPOR-KO mice treated with rhEPO/PL for 1 week.
Means ± SEMs; N numbers in bars; unpaired t tests (2-tailed, 1-tailed in D); scRNA-seq data from 3 mice/group; analyses conducted in area shown in (A).

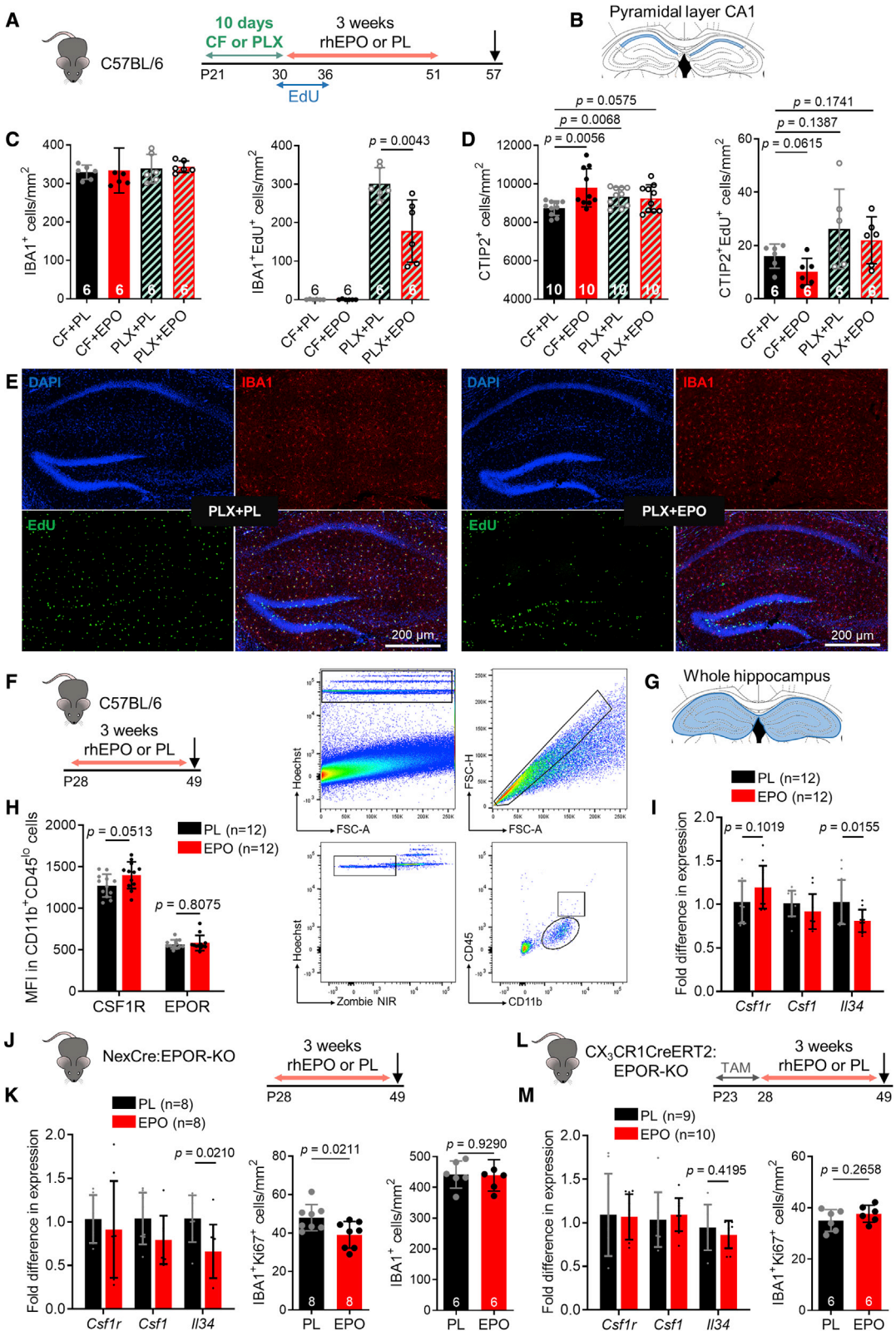

(legend on next page)

et al., 2016), the proliferation of cells in the pyramidal layer was again slightly reduced upon rhEPO. However, no such change was observed after PLX5622 treatment (Figure 3D), perhaps reflecting increased neuronal proliferation under CSF1R inhibition (Elmore et al., 2018). In summary, these findings underline again the counterbalance between microglia and neurons, with rhEPO treatment as well as CSF1R inhibition transiently reducing numbers of proliferating microglia, paralleled by augmented CA1 pyramidal neuron numbers (Figures 3C–3E).

For deeper mechanistic insight, we processed whole hippocampi of 3-week rhEPO or placebo-treated mice (Figures 3F and 3G) to measure the expression of CSF1R and its ligands, CSF1 and interleukin-34 (IL-34). Flow cytometry revealed upregulation of CSF1R expression in $CD11b^{+}CD45^{lo}$ cells upon rhEPO, while EPOR remained unchanged (Figure 3H). The mRNA levels confirmed the trend of increased *Csf1r* expression, while *Csf1* was unaffected. Most important, the neuronally expressed ligand *Il34* (Easley-Neal et al., 2019) was downregulated after rhEPO (Figure 3I). This may suggest that the decrease in *Il34*, as part of a crosstalk between neurons and microglia, adds to containing microglia during EPO-mediated neurodifferentiation.

Since IL-34 is produced by neurons, we explored whether EPO, by binding to hippocampal neurons, could directly decrease *Il34* expression. Hence, we used our NexCre:EPOR-KO mice (Figure 3J) that lack the EPO effect on neuronal differentiation, as reported earlier (Wakhloo et al., 2020). Unexpectedly, *Il34* expression and, consequently, $Ki67^{+}$ microglia numbers remained decreased upon 3 weeks of rhEPO compared to placebo also in NexCre:EPOR-KO mice. In contrast, this decrease did not have a measurable effect on the total number of microglia, which remained unaltered under rhEPO (Figure 3K). This overall unchanged microglia population makes biological sense, considering the lack of increased neurodifferentiation (and thus lack of need for counterbalance) upon pyramidal neuronal EPOR removal. Here, additional yet unexplored factors and pathways could be involved. However, we cannot exclude that continued rhEPO treatment would result at some point in overall reduced microglia in this mutant line. Another possibility to explain these results may be a subset of IL-34-producing neurons, which do not express the Nex (*Neurod6*) promotor, resulting in a fraction of neurons in these mutants that still express EPOR and downregulate *Il34* expression upon EPO. This could lead to a weaker *Il34* reduction that, although detectable, is not strong enough to sustain a decreased microglia population after the initial apoptosis induction.

When we turned for analysis of the same parameters to our $CX_3CR1CreERT2$:EPOR-KO mice again (Figure 3L), we noted to our surprise that the EPO-induced decrease in both *Il34* and proliferating microglia had disappeared (Figure 3M). These data reflect once more that the microglial EPOR plays a primary role in reducing the microglia population and at the same time allows a boost of neurodifferentiation. Future studies will have to answer the question of how microglia, upon EPO binding, signal neurons to decrease their IL-34 production and to elucidate whether this particular microglial-neuronal crosstalk is achieved directly via contact or indirectly via release of soluble factors.

Hypoxia scRNA-seq data support a role of the CSF1R system in the two-wire effect of EPO on microglia and neurogenesis

We now wondered whether similar alterations in the CSF1R axis would be detectable in conditions of hypoxia-induced brain EPO, as demonstrated above (Figures 1A–1D). To address this question, we used our hypoxia scRNA-seq dataset, obtained from whole hippocampus after 5 days of daily exposure to 6% O_2 for 6 h each (Butt et al., 2021b) (Figures 4A and 4B). This dataset allowed us to explore the expression of *Csf1r* and its ligands *Csf1* and *Il34*. In whole hippocampus, we observed, despite their relatively scarce average expression, a mild increase in *Csf1r* (log fold change [logFC] = 0.16) and a mild decrease in *Il34* (logFC = −0.12), whereas *Csf1* was practically unchanged (i.e., log-fold change was close to zero [logFC = 0.04]), indicating basically unchanged levels of *Csf1*, even though statistically significant (Figure 4C). A more detailed look at specific cell populations known to primarily express the respective genes, revealed under hypoxia a marked increase in *Csf1r* expression in microglia (Figure 4D), a negligible increase in *Csf1* in glial cells (Figure 4E), and a mild decrease in *Il34* in glutamatergic neurons (Figure 4F), consistent with our findings by qPCR and flow cytometry following rhEPO treatment. Among the CSF1R ligands, IL-34 is mainly produced by neurons and responsible for microglia maintenance in gray matter areas, as opposed to CSF1, which is mostly expressed by glia and responsible for the maintenance of microglia in white matter regions

Figure 3. Endogenous and exogenous EPO affects microglial proliferation via CSF1R

(A) Treatment scheme for the CSF1R inhibition experiment starting in P21 WT C57BL/6 mice with 10 days of control food (CF) or PLX5622 (PLX), followed by 3 weeks of rhEPO or PL; EdU applied from P30 to P36.

(B) Hippocampal area of analysis.

(C) Quantifications of all $IBA1^{+}$ and proliferating $IBA1^{+}EdU^{+}$ microglia.

(D) Quantifications of all $CTIP2^{+}$ and proliferating $CTIP2^{+}EdU^{+}$ neurons.

(E) Representative images from animals treated with PLX5622 and rhEPO/PL.

(F) Scheme for 3 weeks of rhEPO/PL treatment.

(G–I) Area of analysis (G) for (H) flow cytometry analysis of median fluorescence intensity (MFI) of CSF1R and EPOR in nucleated, single, viable microglial cells ($Hoechst^{+}ZombieNIR^{-}CD11b^{+}CD45^{lo}$ shown in ellipse-shaped gate) and (I) mRNA expression of *Csf1r*, *Csf1*, and *Il34* (normalized to *Hprt1*).

(J) Scheme for 3 weeks of rhEPO/PL treatment in NexCre:EPOR-KO mice.

(K) Whole-hippocampus mRNA expression (normalized to *Hprt1*), $IBA1^{+}Ki67^{+}$, and total $IBA1^{+}$ microglia quantification in mice from (J).

(L) Scheme for 3 weeks of rhEPO/PL treatment in $CX_3CR1CreERT2$:EPOR-KO mice.

(M) Whole-hippocampus mRNA expression (normalized to *Hprt1*) and $IBA1^{+}Ki67^{+}$ microglia quantification in mice from (L); for total $IBA1^{+}$ quantification in these mice see Figure 1M.

Means ± SEMs with N numbers in bars/graphs; qPCR always with 3 technical replicates; all unpaired 2-tailed t tests.

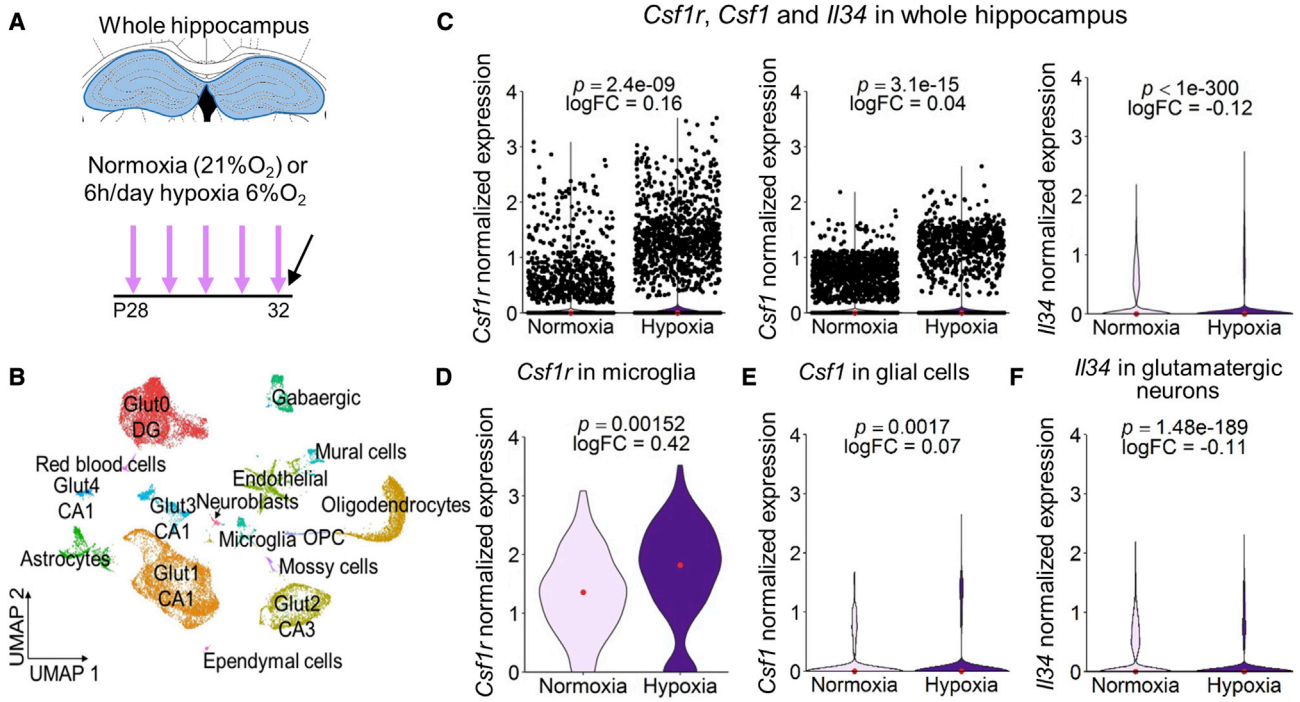

Figure 4. Expression of *Csf1r* and its ligands *Csf1* and *Il34* under hypoxia (scRNA-seq)

(A) Acquisition scheme of scRNA-seq data (Butt et al., 2021b) following normoxia or hypoxia (6% O_2, 6 h/day, 5 days) treatment, and hippocampal area of analysis.

(B) Uniform manifold approximation and projection (UMAP) embedding of cell populations of hippocampus.

(C) Expression of *Csf1r*, *Csf1*, and *Il34* in whole hippocampus.

(D) Expression of *Csf1r* in microglia.

(E) Expression of *Csf1* in glial cells (including microglia, oligodendrocyte progenitor cell [OPC], oligodendrocytes, ependymal cells, and astrocytes).

(F) Expression of *Il34* in glutamatergic neurons.

Bonferroni-corrected p values of correlation-adjusted 2-tailed Mann-Whitney *U* tests in (C)–(F); scRNA-seq data based on 2 mice/group.

(Easley-Neal et al., 2019). The observed decrease in *Il34* expression shown here probably contributes to the counterbalance between neurodifferentiation/numbers of maturing neurons and numbers/activity of microglia under EPO. In fact, glutamatergic neuronal production of *Il34* diminishes after endogenous as well as exogenous EPO, likely to keep the microglia population reduced and less active, while increased neuronal differentiation/maturation proceeds under this growth factor. This explanation is in perfect agreement with the observation that microglia numbers decrease in CA1 after administration of an IL-34 blocking antibody (Obst et al., 2020). The upregulation of *Csf1r* in turn may well be a compensatory homeostatic feedback mechanism in response to decreased *Il34* expression. These data once more imply a role for the CSF1R system in EPO-mediated effects on microglia and neurogenesis.

Working model of a delicate counterbalance between neurodifferentiation and microglia in the adult hippocampal CA1 revealed by EPO

During embryonic development, microglia were reported to assist in the accurate differentiation of CTIP2$^+$ and TBR1$^+$ neurons, and these neuronal subpopulations are dependent on CSF1R signaling for survival (Hattori et al., 2020; Nandi et al., 2012). According to Hattori et al. (2020), "sanctuarization" from microglia in the midembryonic cortical plate is required for neurons to appropriately fine-tune the expression of molecules needed for proper differentiation, thus securing the establishment of functional cortical circuits. Also, in disease models and brain injury studies, decreased microglia proliferation, activity, or motility upon rhEPO treatment has been described, together with improved neuronal proliferation or survival. In fact, rhEPO application in these conditions even prevented neurodegeneration, brain atrophy, and cognitive decline (Mitkovski et al., 2015; Sargin et al., 2009; Sirén et al., 2006; Wang et al., 2017; Zhang et al., 2019).

In contrast, such neurodifferentiation-microglia counterbalance in healthy postnatal and adult CA1 (or anywhere else outside the classical neurogenic niches) has never been reported nor illuminated to understand its physiological significance and underpinnings. Just in the dentate gyrus, the number of microglia was found to be inversely correlated with the number of proliferating progenitor cells in the granule cell layer upon running (Gebara et al., 2013; Kohman et al., 2012). Similarly, reduced numbers or phagocytic capacity of microglia can affect dentate gyrus neurogenesis and neurodifferentiation rates (Diaz-Aparicio et al., 2020; Elmore et al., 2018). Although the phagocytosis of excess neuronal precursor cells is an important mechanism to explain the impact of microglia on neurogenesis (Sierra et al.,

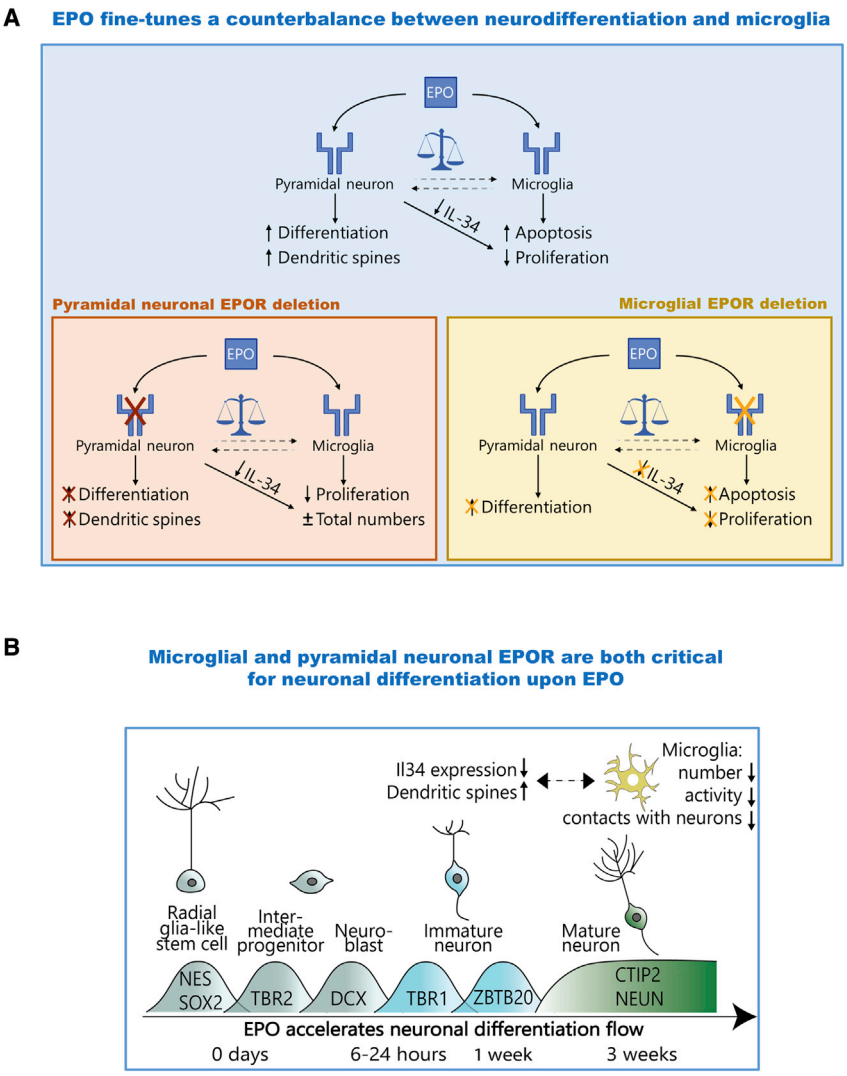

Figure 5. Sketches illustrating the main findings and the resulting working model of the present study

(A) EPO fine-tunes a counterbalance between neurodifferentiation and microglia. Shown on top are the two-wire EPO effects on pyramidal neurons and microglia that maintain a balance between microglia numbers and neurodifferentiation/neuromaturation investigated here. The latter includes dendritic spine formation upon EPO (Wakhloo et al., 2020). Presented at bottom are the resulting alterations upon deletion of pyramidal neuronal EPOR (left) and microglial EPOR (right). Note that the reduced neuronal IL-34 upon EPO is eliminated only upon microglial but not neuronal EPOR deletion, pointing to an involvement of additional signaling pathways from microglia to neurons that depend on microglial EPOR.

(B) Microglial and pyramidal neuronal EPOR are both critical for neuronal differentiation in CA1 upon EPO. This working model suggests that the entire precursor cell lineage in adult murine CA1 that is ready to differentiate toward pyramidal neurons remains "in flow." In the proposed neuronal lineage progression, the EPO-responsive progenitor cells and immature neurons may never constitute abundant clusters in a cross-sectional steady-state analysis, but rather occur in transient waves with individual neurodifferentiation markers rising at particular time windows, as nicely predicted by the pseudotime course and demonstrated here by the quantification of TBR1$^+$ and ZBTB20$^+$ immature neurons (see Figure 2). Elimination of the pyramidal neuronal EPOR eradicates EPO-driven neurodifferentiation (Wakhloo et al., 2020). Strikingly, however, as shown in the present work, upon microglial EPOR deletion, the acceleration by EPO of neuronal differentiation is completely abolished.

2010), it still remains unclear how exactly the reduction in CA1 microglia numbers can enhance neuronal differentiation.

The present work focused on the healthy adult hippocampal CA1 and the role of endogenous and exogenous EPO in coordinating the conduct of different cell types to achieve proper brain hardware upgrade as a prerequisite for improved performance. Thus, as conclusion from the present study, a working model arises, in which the importance of a fine-tuned counterbalance between effective neurodifferentiation and microglia activity in CA1 during normal adulthood is discovered by studying the effects of EPO. This working model defines a two-wire mechanism of this growth factor in the brain, outside the classical neurogenesis areas, and includes CSF1R and its neuronal ligand IL-34 in the way in which the tight regulation of microglia contributes to adult neurogenesis via neurodifferentiation of preexisting precursors (Figures 5A and 5B).

It is tempting to speculate that this two-wire mechanism of EPO may not only be relevant for physiology but also play a beneficial role in pathological states (e.g., upon brain injury or neurodegenerative disease). In fact, elevated IL-34 levels can arise due to neuronal dysfunction and promote a pro-inflammatory environment (Khoshnan et al., 2017; Walker et al., 2017; Wlodarczyk et al., 2019). Our present and previous work suggest that EPO could be a valuable therapeutic aid in circumstances in which microgliosis and increased microglial activation is accompanied by or co-induces neuronal damage. In such situations, EPO can promote via its two-wire effect both neuronal recovery by increasing neurodifferentiation and resolution of inflammation by decreasing microglia numbers and activation.

STAR★METHODS

Detailed methods are provided in the online version of this paper and include the following:

- KEY RESOURCES TABLE
- RESOURCE AVAILABILITY
  - Lead contact

ACKNOWLEDGMENTS

This study was supported by the Max Planck Society, the Deutsche Forschungsgemeinschaft (DFG, German Research Foundation) Research Center for Nanoscale Microscopy and Molecular Physiology of the Brain (CNMPB), and by the DFG grant no. TRR 274/1 2020 - 408885537. A.A.S.-K. has held a stipend of the IMPRS-GGNB Ph.D. Program Neurosciences (DFG grant no. GSC 226), Göttingen. Y.C. is the recipient of a grant from the Peter and Traudl Engelhorn Foundation. U.J.B. has received a PhD stipend from the National University of Sciences and Technology (NUST), Faculty Development Program Abroad 2014/15 Pakistan. J.N. is supported by the Spanish Ministry of Science and Innovation (grant no. RTI2018-098269-B-I00), and K.-A.N. is supported by the Advanced Adelson Medical Research Foundation and an ERC Advanced Grant.

AUTHOR CONTRIBUTIONS

Concept, design, and supervision of the study, H.E. Data acquisition/analysis/interpretation, L.F.G.-A., A.A.S.-K., Y.C., N.B., I.H., S.J., U.J.B., K. Grewe, M.S.W., S.R., J.N., K. Green, K.-A.N., and H.E. Drafting manuscript, L.F.G.-A., A.A.S.-K., Y.C., and H.E. Drafting display items, L.F.G.-A., A.A.S.-K., Y.C., and H.E. All of the authors read and approved the final version of the manuscript.

DECLARATION OF INTERESTS

The authors declare no competing interests.

Received: December 3, 2020
Revised: May 27, 2021
Accepted: July 27, 2021
Published: August 24, 2021

REFERENCES

Adamcio, B., Sargin, D., Stradomska, A., Medrihan, L., Gertler, C., Theis, F., Zhang, M., Müller, M., Hassouna, I., Hannke, K., et al. (2008). Erythropoietin enhances hippocampal long-term potentiation and memory. BMC Biol. *6*, 37.

Allwood, M.A., Romanova, N., Brunt, K.R., and Simpson, J.A. (2017). The Brain, Not the Kidney, is the Source of Erythropoietin in Response to Hypoxic Hypoxia. FASEB J. *31*, 841.816.

Askew, K., Li, K., Olmos-Alonso, A., Garcia-Moreno, F., Liang, Y., Richardson, P., Tipton, T., Chapman, M.A., Riecken, K., Beccari, S., et al. (2017). Coupled Proliferation and Apoptosis Maintain the Rapid Turnover of Microglia in the Adult Brain. Cell Rep. *18*, 391–405.

Badimon, A., Strasburger, H.J., Ayata, P., Chen, X., Nair, A., Ikegami, A., Hwang, P., Chan, A.T., Graves, S.M., Uweru, J.O., et al. (2020). Negative feedback control of neuronal activity by microglia. Nature *586*, 417–423.

Brines, M., and Cerami, A. (2005). Emerging biological roles for erythropoietin in the nervous system. Nat. Rev. Neurosci. *6*, 484–494.

Brown, G., and Ceredig, R. (2019). Modeling the Hematopoietic Landscape. Front. Cell Dev. Biol. *7*, 104.

Butovsky, O., and Weiner, H.L. (2018). Microglial signatures and their role in health and disease. Nat. Rev. Neurosci. *19*, 622–635.

Butt, U.J., Hassouna, I., Fernandez Garcia-Agudo, L., Steixner-Kumar, A.A., Depp, C., Barnkothe, N., Zillmann, M.R., Ronnenberg, A., Bonet, V., Goebbels, S., et al. (2021a). CaMKIIα Expressing Neurons to Report Activity-Related Endogenous Hypoxia upon Motor-Cognitive Challenge. Int. J. Mol. Sci. *22*, 3164.

Butt, U.J., Steixner-Kumar, A.A., Depp, C., Sun, T., Hassouna, I., Wüstefeld, L., Arinrad, S., Zillmann, M.R., Schopf, N., Fernandez Garcia-Agudo, L., et al. (2021b). Hippocampal neurons respond to brain activity with functional hypoxia. Mol. Psychiatry. https://doi.org/10.1038/s41380-020-00988-w.

Cserép, C., Pósfai, B., and Dénes, Á. (2021). Shaping Neuronal Fate: Functional Heterogeneity of Direct Microglia-Neuron Interactions. Neuron *109*, 222–240.

Dagher, N.N., Najafi, A.R., Kayala, K.M., Elmore, M.R., White, T.E., Medeiros, R., West, B.L., and Green, K.N. (2015). Colony-stimulating factor 1 receptor inhibition prevents microglial plaque association and improves cognition in 3xTg-AD mice. J. Neuroinflammation *12*, 139.

Dessypris, E., Graber, S.E., Krantz, S.B., and Stone, W.J. (1988). Effects of recombinant erythropoietin on the concentration and cycling status of human marrow hematopoietic progenitor cells in vivo. Blood *72*, 2060–2062.

Diaz-Aparicio, I., Paris, I., Sierra-Torre, V., Plaza-Zabala, A., Rodríguez-Iglesias, N., Márquez-Ropero, M., Beccari, S., Huguet, P., Abiega, O., Alberdi, E., et al. (2020). Microglia Actively Remodel Adult Hippocampal Neurogenesis through the Phagocytosis Secretome. J. Neurosci. *40*, 1453–1482.

Digicaylioglu, M., Bichet, S., Marti, H.H., Wenger, R.H., Rivas, L.A., Bauer, C., and Gassmann, M. (1995). Localization of specific erythropoietin binding sites in defined areas of the mouse brain. Proc. Natl. Acad. Sci. USA *92*, 3717–3720.

Easley-Neal, C., Foreman, O., Sharma, N., Zarrin, A.A., and Weimer, R.M. (2019). CSF1R Ligands IL-34 and CSF1 Are Differentially Required for Microglia Development and Maintenance in White and Gray Matter Brain Regions. Front. Immunol. *10*, 2199.

Ehrenreich, H., Degner, D., Meller, J., Brines, M., Béhé, M., Hasselblatt, M., Woldt, H., Falkai, P., Knerlich, F., Jacob, S., et al. (2004). Erythropoietin: a candidate compound for neuroprotection in schizophrenia. Mol. Psychiatry *9*, 42–54.

Ehrenreich, H., Hasselblatt, M., Knerlich, F., von Ahsen, N., Jacob, S., Sperling, S., Woldt, H., Vehmeyer, K., Nave, K.A., and Sirén, A.L. (2005). A hematopoietic growth factor, thrombopoietin, has a proapoptotic role in the brain. Proc. Natl. Acad. Sci. USA *102*, 862–867.

Ehrenreich, H., Fischer, B., Norra, C., Schellenberger, F., Stender, N., Stiefel, M., Sirén, A.L., Paulus, W., Nave, K.A., Gold, R., and Bartels, C. (2007a). Exploring recombinant human erythropoietin in chronic progressive multiple sclerosis. Brain *130*, 2577–2588.

Ehrenreich, H., Hinze-Selch, D., Stawicki, S., Aust, C., Knolle-Veentjer, S., Wilms, S., Heinz, G., Erdag, S., Jahn, H., Degner, D., et al. (2007b). Improvement of cognitive functions in chronic schizophrenic patients by recombinant human erythropoietin. Mol. Psychiatry *12*, 206–220.

El-Kordi, A., Radyushkin, K., and Ehrenreich, H. (2009). Erythropoietin improves operant conditioning and stability of cognitive performance in mice. BMC Biol. *7*, 37.

Elmore, M.R., Najafi, A.R., Koike, M.A., Dagher, N.N., Spangenberg, E.E., Rice, R.A., Kitazawa, M., Matusow, B., Nguyen, H., West, B.L., and Green, K.N. (2014). Colony-stimulating factor 1 receptor signaling is necessary for microglia viability, unmasking a microglia progenitor cell in the adult brain. Neuron *82*, 380–397.

Elmore, M.R.P., Hohsfield, L.A., Kramár, E.A., Soreq, L., Lee, R.J., Pham, S.T., Najafi, A.R., Spangenberg, E.E., Wood, M.A., West, B.L., and Green, K.N.

(2018). Replacement of microglia in the aged brain reverses cognitive, synaptic, and neuronal deficits in mice. Aging Cell *17*, e12832.

Gebara, E., Sultan, S., Kocher-Braissant, J., and Toni, N. (2013). Adult hippocampal neurogenesis inversely correlates with microglia in conditions of voluntary running and aging. Front. Neurosci. *7*, 145.

Goebbels, S., Bormuth, I., Bode, U., Hermanson, O., Schwab, M.H., and Nave, K.A. (2006). Genetic targeting of principal neurons in neocortex and hippocampus of NEX-Cre mice. Genesis *44*, 611–621.

Grover, A., Mancini, E., Moore, S., Mead, A.J., Atkinson, D., Rasmussen, K.D., O'Carroll, D., Jacobsen, S.E.W., and Nerlov, C. (2014). Erythropoietin guides multipotent hematopoietic progenitor cells toward an erythroid fate. J. Exp. Med. *211*, 181–188.

Hassouna, I., Ott, C., Wüstefeld, L., Offen, N., Neher, R.A., Mitkovski, M., Winkler, D., Sperling, S., Fries, L., Goebbels, S., et al. (2016). Revisiting adult neurogenesis and the role of erythropoietin for neuronal and oligodendroglial differentiation in the hippocampus. Mol. Psychiatry *21*, 1752–1767.

Hattori, Y., Naito, Y., Tsugawa, Y., Nonaka, S., Wake, H., Nagasawa, T., Kawaguchi, A., and Miyata, T. (2020). Transient microglial absence assists postmigratory cortical neurons in proper differentiation. Nat. Commun. *11*, 1631.

Jelkmann, W. (1992). Erythropoietin: structure, control of production, and function. Physiol. Rev. *72*, 449–489.

Khoshnan, A., Sabbaugh, A., Calamini, B., Marinero, S.A., Dunn, D.E., Yoo, J.H., Ko, J., Lo, D.C., and Patterson, P.H. (2017). IKKβ and mutant huntingtin interactions regulate the expression of IL-34: implications for microglial-mediated neurodegeneration in HD. Hum. Mol. Genet. *26*, 4267–4277.

Kierdorf, K., and Prinz, M. (2017). Microglia in steady state. J. Clin. Invest. *127*, 3201–3209.

Kohman, R.A., DeYoung, E.K., Bhattacharya, T.K., Peterson, L.N., and Rhodes, J.S. (2012). Wheel running attenuates microglia proliferation and increases expression of a proneurogenic phenotype in the hippocampus of aged mice. Brain Behav. Immun. *26*, 803–810.

Krantz, S.B. (1991). Erythropoietin. Blood *77*, 419–434.

Liebetanz, D., and Merkler, D. (2006). Effects of commissural de- and remyelination on motor skill behaviour in the cuprizone mouse model of multiple sclerosis. Exp. Neurol. *202*, 217–224.

Marti, H.H., Wenger, R.H., Rivas, L.A., Straumann, U., Digicaylioglu, M., Henn, V., Yonekawa, Y., Bauer, C., and Gassmann, M. (1996). Erythropoietin gene expression in human, monkey and murine brain. Eur. J. Neurosci. *8*, 666–676.

Miskowiak, K.W., Ehrenreich, H., Christensen, E.M., Kessing, L.V., and Vinberg, M. (2014). Recombinant human erythropoietin to target cognitive dysfunction in bipolar disorder: a double-blind, randomized, placebo-controlled phase 2 trial. J. Clin. Psychiatry *75*, 1347–1355.

Miskowiak, K.W., Vinberg, M., Macoveanu, J., Ehrenreich, H., Køster, N., Inkster, B., Paulson, O.B., Kessing, L.V., Skimminge, A., and Siebner, H.R. (2015). Effects of Erythropoietin on Hippocampal Volume and Memory in Mood Disorders. Biol. Psychiatry *78*, 270–277.

Mitkovski, M., Dahm, L., Heinrich, R., Monnheimer, M., Gerhart, S., Stegmüller, J., Hanisch, U.K., Nave, K.A., and Ehrenreich, H. (2015). Erythropoietin dampens injury-induced microglial motility. J. Cereb. Blood Flow Metab. *35*, 1233–1236.

Nandi, S., Gokhan, S., Dai, X.M., Wei, S., Enikolopov, G., Lin, H., Mehler, M.F., and Stanley, E.R. (2012). The CSF-1 receptor ligands IL-34 and CSF-1 exhibit distinct developmental brain expression patterns and regulate neural progenitor cell maintenance and maturation. Dev. Biol. *367*, 100–113.

Nielsen, J.V., Blom, J.B., Noraberg, J., and Jensen, N.A. (2010). Zbtb20-induced CA1 pyramidal neuron development and area enlargement in the cerebral midline cortex of mice. Cereb. Cortex *20*, 1904–1914.

Nielsen, J.V., Thomassen, M., Møllgård, K., Noraberg, J., and Jensen, N.A. (2014). Zbtb20 defines a hippocampal neuronal identity through direct repression of genes that control projection neuron development in the isocortex. Cereb. Cortex *24*, 1216–1229.

Obst, J., Simon, E., Martin-Estebane, M., Pipi, E., Barkwill, L.M., Gonzalez-Rivera, I., Buchanan, F., Prescott, A.R., Faust, D., Fox, S., et al. (2020). Inhibition of IL-34 Unveils Tissue-Selectivity and Is Sufficient to Reduce Microglial Proliferation in a Model of Chronic Neurodegeneration. Front. Immunol. *11*, 579000.

Ott, C., Martens, H., Hassouna, I., Oliveira, B., Erck, C., Zafeiriou, M.P., Peteri, U.K., Hesse, D., Gerhart, S., Altas, B., et al. (2015). Widespread Expression of Erythropoietin Receptor in Brain and Its Induction by Injury. Mol. Med. *21*, 803–815.

Peskin, A.P., Dima, A.A., Chalfoun, J., and Elliott, J.T. (2010). Predicting Segmentation Accuracy for Biological Cell Images. In ISVC 2010: Advances in Visual Computing, G. Bebis, R. Boyle, B. Parvin, D. Koracin, R. Chung, R. Hammoud, M. Hussain, T. Kar-Han, R. Crawfis, and D. Thalmann, et al., eds. (Springer).

Qiu, X., Mao, Q., Tang, Y., Wang, L., Chawla, R., Pliner, H.A., and Trapnell, C. (2017). Reversed graph embedding resolves complex single-cell trajectories. Nat. Methods *14*, 979–982.

Saka, S.K., Vogts, A., Kröhnert, K., Hillion, F., Rizzoli, S.O., and Wessels, J.T. (2014). Correlated optical and isotopic nanoscopy. Nat. Commun. *5*, 3664.

Sargin, D., Hassouna, I., Sperling, S., Sirén, A.L., and Ehrenreich, H. (2009). Uncoupling of neurodegeneration and gliosis in a murine model of juvenile cortical lesion. Glia *57*, 693–702.

Sargin, D., Friedrichs, H., El-Kordi, A., and Ehrenreich, H. (2010). Erythropoietin as neuroprotective and neuroregenerative treatment strategy: comprehensive overview of 12 years of preclinical and clinical research. Best Pract. Res. Clin. Anaesthesiol. *24*, 573–594.

Schindelin, J., Arganda-Carreras, I., Frise, E., Kaynig, V., Longair, M., Pietzsch, T., Preibisch, S., Rueden, C., Saalfeld, S., Schmid, B., et al. (2012). Fiji: an open-source platform for biological-image analysis. Nat. Methods *9*, 676–682.

Sierra, A., Encinas, J.M., Deudero, J.J., Chancey, J.H., Enikolopov, G., Overstreet-Wadiche, L.S., Tsirka, S.E., and Maletic-Savatic, M. (2010). Microglia shape adult hippocampal neurogenesis through apoptosis-coupled phagocytosis. Cell Stem Cell *7*, 483–495.

Sierra, A., de Castro, F., Del Río-Hortega, J., Iglesias-Rozas, J.R., Garrosa, M., and Kettenmann, H. (2016). The "Big-Bang" for modern glial biology: translation and comments on Pío del Río-Hortega 1919 series of papers on microglia. Glia *64*, 1801–1840.

Sirén, A.L., Fratelli, M., Brines, M., Goemans, C., Casagrande, S., Lewczuk, P., Keenan, S., Gleiter, C., Pasquali, C., Capobianco, A., et al. (2001). Erythropoietin prevents neuronal apoptosis after cerebral ischemia and metabolic stress. Proc. Natl. Acad. Sci. USA *98*, 4044–4049.

Sirén, A.L., Radyushkin, K., Boretius, S., Kämmer, D., Riechers, C.C., Natt, O., Sargin, D., Watanabe, T., Sperling, S., Michaelis, T., et al. (2006). Global brain atrophy after unilateral parietal lesion and its prevention by erythropoietin. Brain *129*, 480–489.

Sirén, A.L., Fasshauer, T., Bartels, C., and Ehrenreich, H. (2009). Therapeutic potential of erythropoietin and its structural or functional variants in the nervous system. Neurotherapeutics *6*, 108–127.

Stuart, T., Butler, A., Hoffman, P., Hafemeister, C., Papalexi, E., Mauck, W.M., 3rd, Hao, Y., Stoeckius, M., Smibert, P., and Satija, R. (2019). Comprehensive Integration of Single-Cell Data. Cell *177*, 1888–1902.e21.

Suresh, S., Rajvanshi, P.K., and Noguchi, C.T. (2020). The Many Facets of Erythropoietin Physiologic and Metabolic Response. Front. Physiol. *10*, 1534.

Wakhloo, D., Scharkowski, F., Curto, Y., Butt, U.J., Bansal, V., Steixner-Kumar, A.A., Wüstefeld, L., Rajput, A., Arinrad, S., Zillmann, M.R., et al. (2020). Functional hypoxia drives neuroplasticity and neurogenesis via brain erythropoietin. Nat. Commun. *11*, 1313.

Walker, D.G., Tang, T.M., and Lue, L.F. (2017). Studies on Colony Stimulating Factor Receptor-1 and Ligands Colony Stimulating Factor-1 and Interleukin-34 in Alzheimer's Disease Brains and Human Microglia. Front. Aging Neurosci. *9*, 244.

Wang, R., Li, J., Duan, Y., Tao, Z., Zhao, H., and Luo, Y. (2017). Effects of Erythropoietin on Gliogenesis during Cerebral Ischemic/Reperfusion Recovery in Adult Mice. Aging Dis. *8*, 410–419.

Wei, S., Nandi, S., Chitu, V., Yeung, Y.G., Yu, W., Huang, M., Williams, L.T., Lin, H., and Stanley, E.R. (2010). Functional overlap but differential expression of CSF-1 and IL-34 in their CSF-1 receptor-mediated regulation of myeloid cells. J. Leukoc. Biol. *88*, 495–505.

Werneburg, S., Feinberg, P.A., Johnson, K.M., and Schafer, D.P. (2017). A microglia-cytokine axis to modulate synaptic connectivity and function. Curr. Opin. Neurobiol. *47*, 138–145.

Wlodarczyk, A., Benmamar-Badel, A., Cédile, O., Jensen, K.N., Kramer, I., Elsborg, N.B., and Owens, T. (2019). CSF1R Stimulation Promotes Increased Neuroprotection by CD11c+ Microglia in EAE. Front. Cell. Neurosci. *12*, 523.

Wustenberg, T., Begemann, M., Bartels, C., Gefeller, O., Stawicki, S., Hinze-Selch, D., Mohr, A., Falkai, P., Aldenhoff, J.B., Knauth, M., et al. (2011). Recombinant human erythropoietin delays loss of gray matter in chronic schizophrenia. Mol. Psychiatry *16*, 26–36.

Xie, Z., Ma, X., Ji, W., Zhou, G., Lu, Y., Xiang, Z., Wang, Y.X., Zhang, L., Hu, Y., Ding, Y.Q., and Zhang, W.J. (2010). Zbtb20 is essential for the specification of CA1 field identity in the developing hippocampus. Proc. Natl. Acad. Sci. USA *107*, 6510–6515.

Zhang, S.J., Wang, R.L., Zhao, H.P., Tao, Z., Li, J.C., Ju, F., Han, Z.P., Ma, Q.F., Liu, P., Ma, S.B., et al. (2019). MEPO promotes neurogenesis and angiogenesis but suppresses gliogenesis in mice with acute ischemic stroke. Eur. J. Pharmacol. *849*, 1–10.

STAR★METHODS

KEY RESOURCES TABLE

REAGENT or RESOURCE	SOURCE	IDENTIFIER
Antibodies		
Chicken anti-IBA1	Synaptic Systems	Cat#234006
Rabbit anti-Ki67	Novocastra	Cat#NCL-Ki67p
Goat anti-caspase-3	Santa Cruz Biotechnology	Cat#sc1225
Guinea pig anti-CTIP2	Synaptic Systems	Cat#325005
Rabbit anti-TBR1	Abcam	Cat#ab183032
Rabbit anti-ZBTB20	Synaptic Systems	Cat#362003
Chemicals, peptides, and recombinant proteins		
Recombinant human EPO (NeoRecormon)	Roche	PZN-04026640
EPREX® buffer	This paper	N/A
Deposited data		
DropSeq EPO-placebo CA1	Wakhloo et al., 2020	GSE144444
10X Genomics hypoxia-normoxia hippocampus	Butt et al., 2021b	GSE162079
Code for scRNaseq analysis	This paper	https://zenodo.org/record/5075213
Experimental models: Organisms/strains		
C57BL/6N mice	Charles Rivers Laboratories	C57BL/6NCrl
$CX_3CR1CreERT2$ mice	Imported from S. Jung	$Cx3cr1^{tm2.1(cre/ERT2)Jung}$
NexCre mice	In-house generated (Goebbels et al., 2006)	$Neurod6^{tm1(cre)Kan}$
EPORflox mice	In-house generated (Wakhloo et al., 2020)	$Epor^{tm1a(KOMP)Wtsi}$
Oligonucleotides		
EPO forward primer: 5′-CATCTGCGACAGTCGAGTTCTG-3′	Allwood et al., 2017	N/A
EPO reverse primer: 5′-CACAACCCATCGTGACATTTTC-3′	Allwood et al., 2017	N/A
Csf1r forward primer: 5′-GCAGTACCACCATCCACTTGTA-3′	This paper	N/A
Csf1r reverse primer: 5′-GTGAGACACTGTCCTTCAGTGC-3′	This paper	N/A
Csf1 forward primer: 5′-CCACATGATTGGGAATGGACAC-3′	This paper	N/A
Csf1 reverse primer: 5′-GATCATCCAGCTGTTCCTGGTCTA-3′	This paper	N/A
Il34 forward primer: 5′-CTTTGGGAAACGAGAATTTGGAGA-3′	Wei et al., 2010	N/A
Il34 reverse primer: 5′-GCAATCCTGTAGTTGATGGGGAAG-3′	Wei et al., 2010	N/A
Hprt1 forward primer: 5′-GCTTGCTGGTGAAAAGGAC CTCTCGAAG-3′	This paper	N/A
Hprt1 reverse primer: 5′-CCCTGAAGTACTCATT ATAGTC AAGGGCAT-3′	This paper	N/A
Software and algorithms		
Fiji	Schindelin et al., 2012	https://imagej.net/software/fiji/
R 4.0.0	R core team, 2020	https://www.R-project.org/
Seurat 3.1.5 (R package)	Stuart et al., 2019	https://cran.r-project.org/web/packages/Seurat/index.html
Monocle 2.16.0 (R package)	Qiu et al., 2017	https://www.bioconductor.org/packages/release/bioc/html/monocle.html
Other		
Complex running wheels (CRW)	TSE Systems	303400-RW
Hypoxia chamber	Coy Laboratory Products	N/A
PLX5622 1200 ppm in AIN-76A standard chow	Research Diets	D19101002S

RESOURCE AVAILABILITY

Lead contact

Further information and requests for resources and reagents should be directed to and will be fulfilled by the lead contact, Hannelore Ehrenreich (ehrenreich@em.mpg.de).

Materials availability

All unique reagents generated in this study are available from the lead contact, Hannelore Ehrenreich (ehrenreich@em.mpg.de).

Data and code availability

- Single-cell RNA-seq data have been deposited at GEO and are publicly available as of the date of publication. Accession numbers are listed in the Key resources table. Microscopy data reported in this paper will be shared by the lead contact upon request.
- All original code has been deposited at Zenodo and is publicly available as of the date of publication. DOI is listed in the Key resources table.
- Any additional information required to reanalyze the data reported in this paper is available from the lead contact upon request.

EXPERIMENTAL MODEL AND SUBJECT DETAILS

Mice

$CX_3CR1CreERT2$ mice were crossed to R26R-tdTomato reporter mice for genetic labeling of microglia ($CX_3CR1CreERT2$:tdTomato) or to EPOR-floxed (Wakhloo et al., 2020) animals to generate conditional EPOR deletion ($CX_3CR1CreERT2$:EPOR-KO). CreERT2 activity was induced with tamoxifen [100 mg/kg intraperitoneal (i.p.) injections over 5 consecutive days, from postnatal day 23 (P23) until P27]. These mice as well as juvenile wild-type (WT) C57BL/6N, Thy1-YFPH and NexCre:EPOR-KO (Goebbels et al., 2006; Wakhloo et al., 2020) mice were treated as indicated in the section 'Treatments' below and in the corresponding figures. All mice used in this work were of male gender [except the cohort for *EPO* mRNA expression in hippocampus (Figures 1A and 1B) and the $CX_3CR1CreERT2$:EPOR-KO mice for 1 week rhEPO treatment (Figure 2P)], and maintained on a 12 h light-dark cycle at 20-22°C, with food and water *ad libitum*.

All experiments were approved by the local Animal Care and Use Committee (Niedersächsisches Landesamt für Verbraucherschutz und Lebensmittelsicherheit) and conducted in accordance with the German Animal Protection Law. In all experiments, investigators were unaware of group assignment or treatment condition ('fully blinded').

Primary microglia culture

Brains from P0-P1 WT C57BL/6N mice were freed from meninges before digestion with trypsin/EDTA 0.05% for 10 min at 37°C. Enzymatic reaction was stopped by adding microglia medium (10% horse serum and 0.5% penicillin/streptomycin in DMEM; all from Invitrogen) supplemented with 400 IU/brain of DNaseI (Worthington Biochemical, Lakewood, NJ, USA). After mechanical trituration, cells were centrifuged (10 min, 150 g) and added to 10 ml pre-warmed microglia medium into poly-D-lysine (PDL)-coated (50 μg/ml) 75 cm^2 cell-culture flask. Cells were incubated at 37°C and 5% CO_2 for 10-14 days. Pure microglia were harvested by manual shaking of flask and seeded in astrocyte-conditioned medium (ACM) at densities of 20,000 cells/well on PDL-coated 12 mm diameter glass-coverslips. ACM was obtained from mixed glial cultures grown in microglia medium for 5-7 days. After 24 h, cells were stimulated with 0.3 or 3 IU/ml EPO or equivalent volume of solvent solution (placebo) for 6 h or 24 h.

METHOD DETAILS

Treatments

For inspiratory hypoxia experiments, mice were put into custom-designed hypoxia chambers (Coy Laboratory Products, Grass Lake, MI, USA) at 6% O_2 for 6 h/day, either once on P32, or on 5 consecutive days from P28 to P32. Other groups were exposed to 12% O_2 for 3 weeks from P28 to P49, starting with gradual reduction of 3% O_2 per day for 3 days. **Complex running wheels** [CRW (Wakhloo et al., 2020); TSE Systems, Bad Homburg, Germany] for voluntary running were placed into normoxia cages for 6 h on P32, or for 3 weeks from P28 to P49. **Recombinant human (rh) EPO** (5000 IU/kg body weight; NeoRecormon, Roche, Welwyn Garden City, UK) or placebo (PL; solvent control solution EPREX® buffer) were applied via i.p. injections (0.01 ml/g) either once or every other day for 1 or 3 weeks as indicated in the treatment schemes of figures, always starting on P28. **For nanoscale secondary ion mass spectrometry (NanoSIMS)**, mice obtained food pellets containing 1.025% L-leucine-^{15}N stable isotope (Sigma-Aldrich, St Louis, MN, USA) for 3 weeks between P28 and P49 (in parallel with EPO/PL injections). **PLX5622** (1200 ppm in AIN-76A standard chow, Research Diets, New Brunswick, NJ, USA) or control food (AIN-76A standard chow), kindly provided by Plexxikon, were given

for 10 days (P21-P30). **EdU** (0.2 mg/ml, Thermo Fisher Scientific, Waltham, MA, USA) was applied via drinking water in light-protected flasks and exchanged on alternate days for the period indicated in schemes.

Quantitative RT-PCR

$CX_3CR1CreERT2$:EPOR-KO and NexCre:EPOR-KO hippocampi were dissected from cryosections (4 sections/mouse) obtained as described in "Immunohistochemistry." RNA of whole hippocampus was extracted using the NucleoSpin totalRNA FFPE Kit (740982, Macherey-Nagel, Düren, Germany) following instructions of the manufacturer. C57BL/6 mice were anesthetized by i.p. injection of Avertin (tribromoethanol, Sigma-Aldrich) and perfused via left cardiac ventricle with Ringer's solution, and RNA of one whole hippocampus per mouse was extracted using miRNeasy Mini Kit (217004, QIAGEN, Hilden, Germany), following instructions of the manufacturer. The cDNA was synthesized using SuperScript III (18080044, Thermo Fisher Scientific); RT-qPCR was performed with Power SYBR Green PCR Master Mix (4367660, Thermo Fisher Scientific). Fold changes in gene expression were calculated with the ΔΔCt method using *Hprt1* as housekeeper. The following primer pairs were used: For *Epo*, forward 5′-CATCTGCGACAGTCGAGTTCTG-3′ and reverse 5′-CACAACCCATCGTGACATTTTC-3′ (Allwood et al., 2017); for *Csf1r*, forward 5′-GCAGTACCACCATCCACTTGTA-3′ and reverse 5′-GTGAGACACTGTCCTTCAGTGC-3′; for *Csf1*, forward 5′-CCACATGATTGGGAATGGACAC-3′ and reverse 5′-GATC ATCCAGCTGTTCCTGGTCTA-3′; for *Il34*, forward 5′-CTTTGGG AAACGAGAATTTGGAGA-3′ and reverse 5′-GCAATCCTGTAGTT GATGGGGAAG-3′ (Wei et al., 2010); and for *Hprt1*, forward 5′-GCTTGCTGGTGAAAAGGACCTCTCGAAG-3′ and reverse 5′-CCCTGAAGTACTCATTATAGTCAAGGGCAT-3′.

Immunohistochemistry

Mice were anesthetized by i.p. injection of Avertin and perfused via left cardiac ventricle with Ringer's solution followed by 4% formaldehyde. The dissected brains were postfixed overnight in 4% formaldehyde and frozen at −80°C after cryoprotection with 30% sucrose. Coronal sections of 30 μm thickness were obtained with cryostat Leica CM1950 (Leica Microsystems, Wetzlar, Germany) and stored at −20°C in 25% ethylene glycol and 25% glycerol in PBS. Following blocking and permeabilization with 5% normal horse serum (NHS) in 0.3% Triton X-100 in PBS (PBST) for 1 h at room temperature (RT), primary antibodies IBA1 (chicken, 1:1000, 234006; Synaptic Systems, Göttingen, Germany), IBA1 (rabbit, 1:1000, ab178846; Abcam, Cambridge, UK), Ki67 (rabbit, 1:1000, NCL-Ki67p; Novocastra, Newcastle Upon Tyne, UK), caspase-3 (goat, 1:250, sc1225; Santa Cruz Biotechnology, Heidelberg, Germany), CTIP2 (guinea pig, 1:1000, 325005; Synaptic Systems), TBR1 (rabbit, 1:500, ab183032; Abcam) and ZBTB20 (rabbit, 1:500, 362003; Synaptic Systems) were incubated in 5% NHS with 0.3% PBST over 2-3 nights at 4°C. Secondary antibodies donkey anti-chicken Alexa Fluor-488 (703546155; Jackson ImmunoResearch, Cambridgeshire, UK), donkey anti-chicken Alexa Fluor-647 (1:500, 703605155; Jackson ImmunoResearch), goat anti-rabbit Alexa Fluor-555 (1:500, A21428; Invitrogen by Thermo Fisher Scientific), donkey anti-guinea pig Cy5 (1:500, 706175148; Jackson ImmunoResearch) donkey anti-guinea pig Alexa Fluor-488 (1:500, 706545148; Jackson ImmunoResearch), donkey anti-rabbit Alexa Fluor-594 (1:500, D-301-C-ABS2; R&D Systems, Wiesbaden, Germany), donkey anti-goat Alexa Fluor-633 (1:500, A21082; Invitrogen) and donkey anti-rabbit Alexa Fluor-488 (1:500, A21206; Invitrogen) were incubated in 3% NHS with 0.3% PBST for 2 h at RT. EdU detection was done with Click-IT EdU Alexa Fluor-647 Imaging kit (C10340; Invitrogen). Cell nuclei were stained with DAPI (1:5000; Millipore-Sigma, Burlington, MA, USA).

NanoSIMS

After immunohistochemistry of the sections, CA1 hippocampal regions were dissected and embedded in LR-White-Resin (AGR1281; Agar Scientific, Wetzlar, Germany) and accelerator mixture (AGR1283; Agar Scientific) following a dehydration protocol as described previously (Saka et al., 2014). Briefly, 30, 50 and 70% ethanol was applied to each section in successive 10-min steps. After drying, sections were brought into a solution containing 70% ethanol and LR-White-Resin. To proceed with resin polymerization, sections were surrounded by a silicon cylinder, and pure LR-White-Resin with accelerator mixture were brought inside of the cylinder. Polymerization was finished after 90 min incubation at 60°C. Sections were further cut into 200 nm thick sections with an EM-UC6 Ultramicrotome (Leica Microsystems) and placed on silicon wafers (Siegert Wafer GmbH, Aachen, Germany). Epifluorescent imaging of IBA1 with a Nikon Ti-E inverted microscope and 100x objective (NA 1.59) was followed by scanning with a Cs^+ primary ion beam in a nanoscale secondary ion mass spectrometry (NanoSIMS 50L) instrument (Cameca, Gennevilliers Cedex, France). Samples were eroded and ionized at 60 pA for 3min, and the measurements were carried out at 2.5 pA with a dwell time per pixel of 4000 ms. From the resulting secondary ions, $^{12}C^{14}N^-$ and $^{12}C^{15}N^-$ were detected and measured, and are referred to as ^{14}N and ^{15}N, respectively, in this work. The mass resolving power was tuned to enable optimal separation of $^{12}C^{15}N^-$ from $^{13}C^{14}N$. For each measurement, 3 planes of 40x40 μm (256x256 pixels) were recorded in a total of 4 animals/group, drift-corrected, and summed for analysis using OpenMIMS-plugin (NRIMS) for ImageJ. The resulting NanoSIMS images were then aligned to corresponding fluorescent images in Adobe-Photoshop. IBA1-positive signals were selected and corresponding NanoSIMS regions quantified in MATLAB (Mathworks, Ismaning, Germany) using a custom written plugin. IBA1-positive regions were normalized to negative ones and compared between conditions in GraphPad Prism8.

Immunocytochemistry

Mixed glial cultures were fixed with 2% acrolein and 3% formaldehyde in PBS, followed by permeabilization and blocking with 5% NHS in 0.1% PBST for 1 h at RT. Primary antibodies IBA1 (chicken, 1:1000, 234006; Synaptic Systems) and caspase-3 (goat, 1:500,

sc1225; Santa Cruz Biotechnologies) were incubated with 1% NHS and 3% BSA in 0.05% PBST overnight at 4°C. As secondary antibodies, donkey anti-chicken Alexa Fluor-488 (703546155; Jackson ImmunoResearch) and donkey anti-goat Alexa Fluor-633 (1:500, A21082; Invitrogen) were used in 1% NHS and 3% BSA in 0.05% PBST for 1 h at RT. Cell nuclei were counterstained with DAPI (1:5000, Millipore-Sigma).

Imaging and analysis

For analysis of IBA1, $CX_3CR1CreERT2$:tdTomato, caspase-3, Ki67, EdU and CTIP2 a Nikon Ti2 Eclipse (Nikon, Tokyo, Japan) epifluorescent microscope with 40x objective (NA0.6) was used. Confocal imaging of IBA1, CTIP2, TBR1 and ZBTB20 was done with Leica TCS-SP5 inverted system equipped with 20x objective (NA0.7), or 40x objective (NA1.25) for morphological analysis of IBA1+ microglia. Image analysis and manual quantifications were done with Fiji (Schindelin et al., 2012) or Imaris v9.1.0 software (Oxford-Instruments, Abingdon, UK) in 3-7 sections/animal (−1.34 to −2.54 mm posterior from Bregma) and in hippocampal regions indicated in figure schemes. For morphological analysis of microglia, the following parameters were obtained with Imaris: filament dendrite length (sum, shown as ''Process length (sum)''), filament full branch level (shown as ''Full branch level''), and filament number of dendrite terminal points (shown as ''Process terminal points''). Perimeter/area ratio was measured in Fiji by outlining the microglial cell body. A maximum of 20 cells/animal were analyzed. For analysis of IBA1 contacts to dendritic spines, a Leica TCS-SPE system with a 63x objective (NA1.4) was used. The number of $IBA1^+$ contacts on principal apical dendrites of Thy1-YFP^+ pyramidal neurons was quantified in average of 17 segments/animal of 50 μm each using Fiji. The segments were randomly selected from the CA1 radiatum layer. Pure microglia cultures were analyzed by imaging 3 different regions of interest (ROIs) in 3 biological replicates (from independent cultures) of 2050x2050 μm (7400x7400 pixels) each.

Flow cytometry

Mice were anesthetized (i.p. Avertin) and perfused via left cardiac ventricle with Ringer's solution. One whole hippocampus per mouse was mechanically dissociated via dounce homogenization in 15 mM HEPES, 0.5% glucose and 1000 IU DNaseI (Worthington Biochemical) in HBSS. After washing, cells were stained with Hoechst3352 (1:500; Thermo Fisher Scientific) and Zombie NIR (1:100, 423105; BioLegend, San Diego, CA, USA). Blocking of Fc-receptors was done with CD16/32 antibody (rat, 1:100, 14016185; Thermo Fisher Scientific) in fluorescence-activated cell sorting (FACS) buffer (2% FCS, 0.01M EDTA pH8.0 and 0.01% NaN_3 in PBS). Primary antibodies CD11b Alexa Fluor-488 (rat, 1:100, 53011282; eBioscience by Thermo Fisher Scientific) and CD45 PerCP-Cy5.5 (rat, 1:100, 103132; BioLegend) in FACS buffer were used in extracellular staining for microglia identification. After fixation and permeabilization with commercially available solutions (775775, Invitrogen), intracellular staining with CSF1R PE (rat, 1:100, 135505; BioLegend), EPOR (rabbit, 1:250, SA7378; Synaptic Systems) and donkey anti-rabbit Alexa Fluor-594 (1:250, A21207; Invitrogen) was done in 0.1% saponin, 1% BSA and 5% NHS in PBS. Fluorescent minus one controls were processed in parallel. Filtered samples were acquired on BD-LSR-Fortessa (BD-Biosciences, San Jose, CA, USA) and data was analyzed in FlowJo software (BD Biosciences).

Single cell RNA sequencing

Single cell RNA sequencing (scRNA-seq) data was obtained and processed as described in detail earlier (GSE144444 [Wakhloo et al., 2020] and GSE162079 [Butt et al., 2021b]).

Data deposited under GSE144444 were derived from CA1 tissue which was extracted from 3 mice/group (P28) 6 hours after treatment with a single EPO or placebo injection. Single cell suspensions were barcoded using a FlowJEM aquapel-treated DropSeq microfluidic device (FlowJEM). After reverse transcription, cDNA libraries were amplified and subsequently sequenced with Illumina HiSeq 2500. Data processing was performed using R (v3.4.1) packages Seurat v2.3.0 (quality control, normalization, integration, clustering) and Monocle v2.16.0 (pseudotemporal ordering/trajectory analysis, temporal differential expression testing). The total dataset consisted of 14,061 genes in 390 cells from placebo and 14,971 genes in 583 cells from the EPO group. For trajectory analysis two clusters of glutamatergic cells, 'Immature Glutamatergic' and 'Mature Glutamatergic1' (N = 502 cells), representing different stages of maturation, were subset and analyzed. In order to identify neuronal genes characteristic of an intermediate stage of maturity, differential expression testing was performed by contrasting cells with a pseudotime within or outside the range of 3-25 using the monocle function differentialGeneTest. Top 30 candidate genes (sorted by p value) were initially screened for expression patterns that indicated temporal upregulation during maturation and matched literature reports. The best candidate (*Zbtb20*) was selected for immunohistochemistry.

Data deposited under GSE162079 were generated from 2 mice/group, exposed to either normoxia or hypoxia (6% O_2/6h per day) for five consecutive days (from P28 to P32). Hippocampi were isolated and generated single cell suspensions stored at −80°C until further processing. Barcoding and cDNA libraries were prepared using 10X Genomics v2 chemistry. Resulting librariers were sequenced on Illumina HiSeq 4000. Alignment was performed using CellRanger v2.2.0. Sample quality control, normalization, integration and clustering was performed in R (v3.4.1) using the Seurat package (v2.3.0 and v.3.0.0). The final dataset contained 25,850 cells (normoxia: N = 12,341, hypoxia: N = 13,509) and 20,976 genes. Differential expression analysis of *Csf1r*, *Csf1* and *Il34* was executed using Seurat's FindMarkers function.

QUANTIFICATION AND STATISTICAL ANALYSIS

Data is shown as mean ± standard error of the mean (SEM), with N numbers (i.e., number of mice/group) and statistical tests specified in the text or corresponding figure legend. *In vitro* data represent triplicate measurements from 3 independent cultures (biological replicates). Statistical analyses were performed with GraphPad Prism5 or R4.0.0. Student's unpaired two- or one-tailed t tests were performed in normally distributed data and two-tailed Mann-Whitney *U* test in non-parametric data. Differential expression analysis (scRNA-seq, whole hippocampus) was performed using the FindMarkers() function in Seurat-3.1.5 (Stuart et al., 2019) (two-tailed correlation-adjusted Mann-Whitney *U* test). Reported p values were adjusted for total number of genes (n = 18976) expressed in the dataset. Differential expression-testing used to identify intermediate neuronal markers on pseudotime trajectory (scRNA-seq, CA1) was performed in Monocle-2.16.0 (Qiu et al., 2017), using the function differentialGeneTest(), and false-discovery rate adjusted p values were reported.